arXiv:0811.1753v1 [astro-ph] 11 Nov 2008

The X-Ray Environment During the Epoch of Terrestrial Planet Formation: Chandra Observations of h Persei

Thayne Currie[1], Nancy Remage Evans[1], Brad D. Spitzbart[1], Jonathan Irwin[1], Scott J. Wolk[1], Jesus Hernandez[2,4], Scott J. Kenyon[1], and Jay M. Pasachoff[3]

tcurrie@cfa.harvard.edu

ABSTRACT

We describe Chandra/ACIS-I observations of the massive $\sim$ 13–14 Myr-old cluster, h Persei, part of the famous Double Cluster (h and χ Persei) in Perseus. Combining the list of Chandra-detected sources with new optical/IR photometry and optical spectroscopy reveals $\sim$ 165 X-ray bright stars with V $\lesssim$ 23. Roughly 142 have optical magnitudes and colors consistent with cluster membership. The observed distribution of L_x peaks at $L_x \sim 10^{30.3}$ ergs s^{-1} and likely traces the bright edge of a far larger population of $\approx$ 0.4–2 $M_\odot$ X-ray active stars. From a short list of X-ray active stars with IRAC 8 μm excess from warm, terrestrial-zone dust, we derive a maximum X-ray flux incident on forming terrestrial planets. Although there is no correlation between X-ray activity and IRAC excess, the fractional X-ray luminosity correlates with optical colors and spectral type. By comparing the distribution of $L_x/L_\star$ vs. spectral type and V-I in h Per with results for other 1–100 Myr-old clusters, we show that stars slightly more massive than the Sun ($\gtrsim$ 1.5 $M_\odot$) fall out of X-ray saturation by $\approx$ 10–15 Myr. Changes in stellar structure for $\gtrsim$ 1.5 $M_\odot$ stars likely play an important role in this decline of X-ray emission.

Subject headings: stars: pre-main-sequence–planetary systems: formation — planetary systems: circumstellar disks — Open Clusters and Associations:Individual: NGC 869

Facility: Chandra X-Ray Observatory, Kitt Peak National Observatory, MMT Observatory, Spitzer Space Telescope

[1]Harvard-Smithsonian Center for Astrophysics, 60 Garden St. Cambridge, MA 02140

[2]Department of Astronomy, University of Michigan

[3]Department of Astronomy, Williams College

[4]Centro de Investigaciones de Astronomía, Apdo Postal 264, Merida 5101-A, Venezuela

1. Introduction

Intermediate and low-mass main sequence stars like the Sun show evidence for chromospheric/coronal activity. Diagnostics of this activity – Ca II H and K emission, X-ray emission, etc. – are likely produced from a self-sustaining magnetic dynamo, which results from a combination of convective energy transport and differential rotation (Parker 1955; Babcock 1961; Barnes 2003). Once stars begin to contract onto the main sequence, the X-ray luminosity (L_x) correlates with stellar rotation (v), with $L_x \propto v^2$ (Pallavicini et al. 1981; Güdel et al. 1997). This evolution provides a quantifiable link between a major diagnostic of activity and the source of activity (see also Pizzolato et al. 2003). Therefore, studying the evolution of X-ray emission provides an insight into stellar structure and evolution and the influence of activity on the circumstellar environment.

Young analogs of main sequence field stars have much higher levels of X-ray emission than main sequence stars. X-ray surveys of young, $\lesssim 100$ Myr-old open clusters reveal that intermediate mass ($\sim$ 1-3 $M_\odot$) and low-mass stars are strong X-ray emitters. Typical X-ray luminosities for young stars are $\sim$ 100-1,000 times larger than the characteristic solar X-ray luminosity (Feigelson et al. 2005; Preibisch and Feigelson 2005; Preibisch et al. 2005).

X-ray observations of clusters (e.g. with Chandra) provide detailed constraints on the time history of chromospheric activity. As stars age and evolve onto the main sequence, their magnetic activity diminishes. Thus, their X-ray luminosity declines (Skumanich 1972; Micela et al. 1985; Güdel et al. 1997; Feigelson and Montmerle 1999; Evans and Seward 2000; Preibisch and Feigelson 2005). This decay is likely due to the rotational spin-down of the star and reduction of differential rotation at the radiative/convective zone interface (e.g. Noyes et al. 1984; Baliunas et al. 1995). The youngest ($\sim$ 1 Myr old) stars less massive than $\sim$ 1-2 $M_\odot$ typically have $L_x \sim 10^{29}$–10^{31} ergs s^{-1} and fractional luminosities ($L_x/L_\star$, where $L_\star$ is the bolometric luminosity) of $\sim 10^{-3}$–10^{-4} (Preibisch and Feigelson 2005). Observations of older clusters like the Pleiades (Micela et al. 1999) suggest that the typical X-ray luminosities drop to 10^{29} ergs s^{-1} and fractional luminosities drop to $\sim 10^{-4}$–$10^{-4.5}$ by 100 Myr.

Observations of young stars also show that a stellar mass dependence of X-ray emission emerges sometime after $\approx$ 2 Myr. In the COUP observations of the Orion Nebula Cluster, young stars have a wide range of fractional luminosities which are not correlated with stellar mass (Preibisch and Feigelson 2005; Preibisch et al. 2005). X-ray activity from the magnetic dynamo is uncorrelated with rotation rate and is described as being "saturated", $L_x/L_\star \sim 10^{-3}$, or "supersaturated", $L_x/L_\star > 10^{-3}$ (Randich et al. 1996; Güdel 2004). In contrast, observations of older clusters like the Pleiades suggest clear relations between $L_x/L_\star$ and stellar mass (Micela et al. 1999), where lower-mass stars have a higher fractional luminosity.

Thus, sometime between 1 Myr and 100 Myr, stellar rotation rates decrease sufficiently to bring the X-ray activity out of saturation (Patten and Simon 1996; Güdel 2004).

As stars evolve to the main sequence, their X-ray emission may drive important processes in the circumstellar disk material from which planets form. X-ray active stars with ages of $\sim$ 1-10 Myr are surrounded by primordial circumstellar disks comprised of gas and small dust grains (Kenyon and Hartmann 1995). X-ray irradiation may provide an ionization source for primordial disks that powers disk viscosity to sustain disk accretion when MRI turbulence is otherwise ineffective (Glassgold, Najita, and Igea 1997). Flash heating from X-rays in powerful solar flares may account for the formation of chondrules in the early solar nebula (Shu et al. 1996). X-ray heating of solids during flaring events, perhaps even during the early debris disk stage, may also drive chemical reactions from spallation which produces the short-lived isotopes observed in some meteorites (Feigelson et al. 2002).

X-ray irradiation also has important consequences for the evolution of newly-formed planets. Large X-ray fluxes can ablate the hydrogen-rich atmospheres of short-period giant planets (Lammer et al. 2003) and remove the atmosphere entirely for sufficiently high L_x (see also Baraffe et al. 2004). For an X-ray luminosity function scaled to the Pleiades, nearly all ($\sim$ 85%) Neptune-mass gaseous planets at 0.02 AU from a solar-type star may be eroded to Super-Earths (Penz et al. 2008). G-type stars with high X-ray luminosities can evaporate the atmospheres of a wide range of planet masses ($\sim$ 0.1-10 $M_\oplus$) within $\sim$ 0.1 AU. In the absence of evaporation, X-ray irradiation may also drive a variety of photochemical reactions in the atmospheres of terrestrial planets (e.g. Lammer et al. 2007).

Understanding the evolution of stellar activity and the X-ray environment of circumstellar disks and planets requires observations of stars in clusters with ages of $\approx$ 10–30 Myr. Recent X-ray surveys have concentrated on $\lesssim$ 5 Myr-old clusters such as Orion, NGC 2264, and IC 348 and $\gtrsim$ 50–100 Myr old clusters such as α Persei and the Pleiades (Prosser et al. 1996; Micela et al. 1999; Preibisch and Zinnecker 2002; Preibisch and Feigelson 2005; Dahm et al. 2007). The large gap in ages between the youngest and the oldest clusters makes it difficult to constrain the evolution of the X-ray luminosity function and the evolution of stellar activity. X-ray data for 10–30 Myr-old clusters also link constraints on the X-ray environment during accretion and grain growth in the primordial disk phase with those for $\gtrsim$ 100 Myr-old stars where planet formation should be complete in the terrestrial zone.

In this paper, we report analysis of Chandra observations of 13–14 Myr old h Persei, part of the famous Double Cluster h and χ Persei. Recent Spitzer observations of h Persei (Currie et al. 2007a, 2008a; Currie 2008b) reveal that the cluster harbors a substantial population of stars with warm dust emission consistent with debris from active terrestrial planet formation (Currie et al. 2007b; Currie 2008b). At $\sim$ 13-14 Myr (Slesnick et al. 2002;

Meynet et al. 1993; Currie 2008b), h Persei probes ages during which terrestrial planets are potentially in the final stages of formation (Kenyon and Bromley 2006; Wetherill and Stewart 1993) and when nebular gas has recently dissipated (Currie et al. 2007c, see also Thommes, Matsumura, and 2008 and references therein), leaving newly-formed gas giants unshielded from high energy X-ray photons.

Our main goals for this paper are twofold. First, we investigate the connection between X-ray activity and warm debris emission. For X-ray bright stars with evidence for warm dust, we estimate an X-ray flux in the terrestrial zone that provides input for planetary atmosphere evaporation models. Second, we provide constraints on the time-evolution of stellar X-ray activity linking studies of younger $\sim$ 1–2 Myr-old clusters like Orion and older clusters like the Pleiades. Chandra sensitivity limits likely preclude sampling the full distribution of X-ray active stars in h Persei. However, we can analyze the upper envelope of the distribution of L_x and $L_x/L_\star$ as a function of stellar properties. From comparing the bright limit of the $L_x/L_\star$ distribution from h Per with the distribution from younger and older clusters, we look for evidence of evolution in stellar activity. A detailed investigation of the X-ray spectra for sources with the highest X-ray counts will be included in future work (N. Evans et al., in prep.)

2. Chandra Observations and Ancillary Data

2.1. Observations, Image Processing, and Source Extraction

Chandra observations of h Persei were taken with a 41.1 ksec exposure on Dec. 2, 2004 (Obs. ID 5407; Sequence Number 200341) with the ACIS detector (chips 0, 1, 2, 3, 6, and 7; Weisskopf et al. 2002). The data were obtained in dithered, timed mode, with a frametime of 3.2 seconds. On-board event rejection and event telemetry was in VFAINT mode. The field was centered on $\alpha_{2000}=2^h19^m00^s$, $\delta_{2000}=57^o07'12"$, close to the center of h Persei from Bragg and Kenyon (2005) ($\alpha_{2000}=2^h18^m56.4^s$, $\delta_{2000}=57^o08'25"$) and observed at a roll angle of 229°. The data were not registered to an astrometric reference frame (e.g. 2MASS). The ACIS-I field covers a 17'x17' area.

Figure 1 shows the reduced, smoothed image, binned by 4 pixels and then convolved with a 3 pixel gaussian to balance the prominence of the sources in the center of the field with those on the edges. On the original data (which is the basis for all further analysis) the sources in the center of the field are smaller than sources on the edge where the point spread function (psf) is larger.

We process the images with the standard ANCHORS (An Archive of Chandra Ob-

servations of Regions of Star Formation) pipeline (`http://cxc.harvard.edu/ANCHORS/`; Spitzbart et al. 2008). Based on the CIAO (Chandra Interactive Analysis of Observations) routines, this reduction system is designed to process Chandra images containing many point sources and diffuse emission. The CXC pipeline level 2 data products (DS version 7.6) required no reprocessing; we only applied an energy filter at 0.3–8.0 keV to eliminate the high-energy background.

To select X-ray sources, we investigated several source detection algorithms available in CIAO. We used a recursive blocking scheme with WAVDETECT (Freeman et al. 2002, Mexican hat wavelet detection) with the significance set to yield about 1 false detection per field. A 15'x15' region centered on the aimpoint was extracted at full resolution. WAVDETECT then identified sources in this region using wavelet scales of 2, 4, 8, 16, and 32. We merged the three lists, removing any duplicates.

This method yields 330 point source detections. Source positions were then adjusted using a centroiding routine. We extracted counts using an elliptical extraction region around each source based on point-spread function fitting as a function of chip position at 95% encircled energy. Background levels were computed using an annular ellipse with the same shape as the source extraction. The outer ellipse boundry has major and minor axes six times the size of the source; the inner boundry has axes three times the size of the source.

2.2. Deriving the X-Ray Flux and Temperature

We derived the X-ray flux and temperature for each Chandra source using a one temperature APEC model with absorption using the CIAO fitting and modeling package Sherpa, v. 3.4[1]. Unless X-ray sources are very strong (100 counts or more), it is useful to fix several parameters in the fits to prevent unphysical values. The fixed parameters are the hydrogen column density, n_H, the initial X-ray temperature, and the abundance parameter.

We use the well-constrained reddening of h Persei to set n_H. Based on $\sim$ 100 high-mass stars, Slesnick et al. (2002) derive E(B-V) $\sim 0.56 \pm 0.01$, a value within 10% of estimates from similar work (e.g. Keller et al. 2001; Bragg and Kenyon 2005) and identical to that derived for χ Persei. From optical spectroscopy of $\sim$ 6,000 stars, Currie (2008b) and Currie et al. (2008c) derive E(B-V) ~ 0.56 for both h and χ Persei. Currie (2008b) identifies a full-width half-maximum of ~ 0.1 in the distribution of E(B-V). Very few cluster stars have E(B-V) $\gtrsim 0.65$ or $\lesssim 0.45$. Because E(B-V) is proportional to n_H, adopting a single

[1]http://cxc.harvard.edu/sherpa3.4/index.html/

$n_H \approx 3 \times 10^{21}$ cm^{-2} for E(B-V) $\sim$ 0.56 introduces a $\approx$ 10% uncertainty in n_H and a $\approx$ 0.05 dex uncertainty in log(L_X) for each source. Additionally, there is a $\approx$ 10% systematic uncertainty as we chose a constant of proportionality for the E(B-V) to N_H relation which is intermediate between the values of Vuong et al. (2003) and Ryter et al. (1996).

We adopted an initial temperature kT of 1.5 keV as a compromise between values typical of stars in younger clusters (e.g. M17, Broos et al. 2007) and stars in older clusters (e.g. the Pleiades, Daniel, Linsky, and Gagne 2002). An abundance parameter of 0.3 solar is routinely found in fits of X-ray spectra and assumed constant in our calculations (Feigelson et al. 2002). The n_H and abundance parameters remain fixed throughout the fitting, while kT is determined from fitting. The remaining free parameter is the normalization from which Sherpa derives both the absorbed and unabsorbed photon fluxes.

We performed a two-step fitting procedure. First, the unbinned data were fitted using C-statistics (Cash 1979) and Powell optimization (identifies local fit statistic minimum nearest to initial guess. For sources with more than 30 counts, the data were then grouped for 8 counts/bin and refit using the result from the unbinned fit as an initial guess for the normalization and temperature. The binned fitting used χ-dvar statistics and Levenberg-Marquardt optimization. The details of these optimization methods are described in the online Sherpa documentation[2].

Table 1 lists data for Chandra-detected sources. Column 1 is the source ID, columns 2 and 3 list J2000 positions, columns 4 and 5 list the raw and net counts in the 95% encircled energy radius. The hardness ratios (columns 6–8) describe the energy of X-ray photons. Following Getman et al. (2005), we use three hardness ratios. HR1 compares the full range of CXO sensitivity: 0.5–2.0 keV vs. 2.0–8.0 keV. HR2 highlights differences in the softer region (0.5–1.7 keV vs. 1.7–2.8 keV), while HR3 highlights differences in the harder regions (1.7–2.8 keV vs. 2.8–8.0 keV). Columns 10 and 11 list the X-ray temperature and uncertainty in temperature. Although a detailed analysis of the X-ray spectra is the subject of future work (N. Evans et al., in prep.), the median X-ray temperature for the entire sample is $\sim$ 1.6 keV, which is reasonable for stars with ages intermediate between $\sim$ 1 Myr and 100 Myr as described in §2.2. Columns 12 and 13 list the derived unabsorbed and absorbed X-ray fluxes. The median values for the unabsorbed and absorbed fluxes are $10^{-14.6}$ ergs cm^{-2} s^{-1} and $10^{-14.8}$ ergs cm^{-2} s^{-1}. The reduced χ^2 of the Sherpa fits are listed in column 14.

[2]http://cxc.harvard.edu/sherpa/methods/methods.html

2.3. Optical/IR Ancillary Data

There are several possible types of X-ray active sources on the Chandra field, including chromospherically active pre-main sequence stars, active galactic nuclei (AGN), and foreground/background red giant stars. Without useful proper motion data for this distant cluster, we rely on optical/infrared colors and deep Chandra number counts (e.g. Bauer et al. 2004) to identify likely cluster members and to make plausibility arguments for sources without optical IDs. For populous clusters like h and χ Persei, we expect a well-defined locus in an optical color-magnitude diagram (e.g. Lyra et al. 2006). The optical luminosities for young (e.g 10–50 Myr) intermediate/late spectral type pre-main sequence stars (e.g. G0-M5) are up to ≈ 5 times greater than their main sequence field star counterparts (e.g. Baraffe et al. 1998). Thus, field stars have far bluer colors at a given magnitude. Background AGN have very blue optical colors compared to pre-main sequence stars and have very faint optical magnitudes. Foreground red giant stars have far redder colors than cluster stars at a given magnitude. The differences in V/V-I positions for cluster stars and other X-ray active sources means that this color-magnitude diagram clearly identifies the positions of X-ray active cluster members in moderately massive clusters such as NGC 2547 (Lyra et al. 2006). Because h Persei is $\gtrsim$ 5–10 times more massive than NGC 2547, the cluster locus should be even more easily identifiable.

To identify the nature of Chandra-detected sources, we merged the Chandra catalog with deep VI optical photometry and optical spectra of h Persei[3]. Optical photometry of h Persei was taken with the Mosaic Imager at the 4-meter Mayall telescope at the Kitt Peak National Observatory on October 13-16 and 27-30, 2006, as a part of the MONITOR project (Aigrain et al. 2007). Exposures in V and I band were taken using 75 second integrations with a 36'x36' field of view centered on the cluster. The data were reduced using the pipeline for the INT wide-field survey (Irwin and Lewis 2001; Irwin et al. 2007), correcting for the effects of fringing, cross talk, bias, and atmospheric extinction. Photometry was performed as in Irwin et al. (2007); instrumental magnitudes were transformed into Johnson-Cousins system magnitudes. The catalog contains $\approx$ 42,000 sources detected in at least one band and are complete at the 5σ level to V $\sim$ 23 and I $\sim$ 20.

For source matching, we use the optical photometry. For 14 Myr-old cluster stars at the distance and reddening of h Per (E(B-V) $\sim$ 0.56; d $\sim$ 2.3–2.4 kpc Slesnick et al. 2002; Currie et al. 2008c), stars with J-band magnitudes brighter than the 2MASS completeness limit (J $\sim$ 15.7) have V-I $\lesssim$ 1.75, V-J $\lesssim$ 3.3, and V $\lesssim$ 19 (Kenyon and Hartmann 1995;

[3]The optical photometry and spectroscopy presented in this section will be discussed in more detail in an upcoming paper (Currie et al. 2008c).

Baraffe et al. 1998; Siess et al. 2000). Cluster stars with V $\sim$ 23 (the 5σ limit for our optical data) have V-I $\sim$ 3, V-J $\sim$ 4.5, and J $\lesssim$ 18.5 (cf. Kenyon and Hartmann 1995). Thus, the optical data detect fainter, lower-mass cluster stars than the 2MASS data.

To provide more constraints on the properties of optically-detected Chandra sources, we include optical spectra of h Per sources. Optical spectroscopy of $\approx$ 5,000 h Persei sources were taken during Fall 2006 and Fall 2007 with Hectospec (Fabricant et al. 2005) on the 6.5m MMT telescope. We took three 10-15 minute exposures using the 270 g mm^{-1} grating. This configuration yields spectra at 4000-9000 Å with 3 Å resolution. The data were processed using standard Hectospec reduction pipelines. The reduced spectra typically had signal-to-noise $\gtrsim$ 20-40. Finally, we include $\sim$ 1000 archival spectra from the FAST and Hydra spectrographs on the 1.5 m Tillinghast and 3.5 m WIYN telescopes, respectively. Currie et al. (2007b) and Currie (2008b) describe these data in detail. The FAST and Hydra spectra consist mostly of bright, likely early-type stars in h Persei.

To derive spectral types from these spectra, we employed the semi-automatic quantitative spectral-typing code **SPTCLASS** from Hernandez et al. (2004, see www.astro.lsa.umich.edu/hernandj for more information), which is useful for classifying stars regardless of luminosity class and surface gravity. **SPTCLASS** calculates the spectral types of stars using spectral indices which compare the line flux of each spectral feature to continuum levels. The relationships between spectral indices and spectral types are derived from spectroscopic standards observed with Hectospec. Thus, **SPTCLASS** is particularly well suited to spectral type h Persei stars. The errors in spectral types are typically $\approx$ 2 subclasses.

To identify the presence or absence of warm, circumstellar dust around X-ray active stars, we match ACIS sources to the 2MASS/IRAC catalog from Currie et al. (2007a). Currie et al. (2007a) describe the data reduction, photometry, and source matching between 2MASS and IRAC in detail. The catalog consists of $\sim$ 31,000 point sources and covers $\approx$ 0.75 square degrees on the sky, encompassing both h Persei and χ Persei. The completeness limit for the catalog corresponds to the 2MASS completeness limit (J $\approx$ 15.5); most stars brighter than J $\sim$ 15-15.5 have IRAC counterparts in at least one channel (3.6 μm, 4.5 μm, 5.8 μm, or 8 μm).

Of the 330 X-ray sources, 165 have optical photometric counterparts. The typical positional offsets are very small (mean offset is $\sim$ 0.60", median $\sim$ 0.47", and $\sigma \sim$ 0.43") and comparable to the astrometric accuracy of Chandra. Of the 165 X-ray/optically-detected sources, 101 have spectral types; 123 have also 2MASS/IRAC photometry. We derive the X-ray luminosity for optically-detected Chandra sources assuming a distance of 2.4 kpc.

The catalog of optically-detected Chandra sources along with their net X-ray counts

and absorption-corrected X-ray luminosities[4], optical/IR photometry, and spectral types is listed in Table 2[5].

2.4. Nature of Chandra Sources Lacking Optical Detections

By comparing the optical survey limits to colors and magnitudes for 14 Myr-old pre-main sequence stars and other X-ray active sources we can constrain the properties of Chandra sources lacking optical detections. The two main possibilities for these sources are fainter, low-mass cluster stars and background AGN. Simple arguments show that both fainter, low-mass cluster stars and AGN likely comprise the Chandra-detected population lacking optical detections.

For the Geneva/Baraffe isochrone (see §3.1), stars with V $\sim$ 22 have masses of $\sim$ 0.6 $M_\odot$ (Figure 2). While model uncertainties plague our understanding of the optical colors/magnitudes of lower-mass stars, these stars should be cooler and fainter than 0.6 $M_\odot$ stars of the same age. Baraffe et al. (1998) predict that h Per stars with $M_\star \sim 0.25$ $M_\odot$ have V $\sim$ 24, two magnitudes fainter than 0.6 $M_\odot$ stars and undetectable with our optical data. If these stars have high fractional x-ray luminosities ($\geq 10^{-3}$, Chandra is likely sensitive enough to detect them. Because the 5σ limit for the optical data is V $\sim$ 23, stars of slightly greater mass ($\lesssim$ 0.5 $M_\odot$) may also lack optical detections but have Chandra detections.

Assuming a Miller-Scalo Initial Mass Function (Miller and Scalo 1979), h Per stars with masses between 0.25 $M_\odot$ and 0.6 $M_\odot$ are 1.3 times as numerous as cluster stars with masses $\gtrsim$ 0.6 $M_\odot$. The number of optically-detected Chandra sources is equal to the number lacking optical detections. Therefore, lower-mass cluster stars plausibly comprise a significant fraction of the Chandra-detected population lacking optical detections.

Using the number counts of X-ray sources as a function of limiting flux from Bauer et al. (2004), Chandra sources lacking optical detections likely include a significant population of optically faint, background AGN. The limiting (unabsorbed) flux for our survey is log(F_x, ergs s^{-1} cm^{-2}) $\approx$ -14.7. Bauer et al. (2004) derive the number of X-ray sources per sq deg with fluxes greater than log (F_x ergs s^{-1} cm^{-2}) = -14.7 to be roughly 500 soft X-ray sources and 1000 hard X-ray sources. Because the ACIS-I coverage is $\approx$ 0.08 square degrees, our h Per field should have $\sim$ 40 (80) soft (hard) AGN. Most AGN with log $F_x \sim -14.7$ have faint optical magnitudes (R $\gtrsim$ 22–23; Bauer et al. 2004) and are thus fainter than the 5 σ limit

[4]All X-ray luminosities discussed in the following sections are *absorption-corrected* luminosities

[5]The full versions of the tables are available in the electronic edition of this paper

of our optical survey.

Other properties of sources with and without optical Several X-ray sources on the field have 2MASS detections but no detectable optical counterparts. These are typically very faint and do not define a locus in near-IR color-magnitude diagrams consistent with cluster membership. These sources are then more likely to be AGN.

In summary, the Chandra sources lacking optical counterparts are likely to be a mix of low-mass cluster stars and background AGN. Deeper optical data will likely identify the origin of some currently unmatched sources. Deeper X-ray data will yield enough counts to fit a spectrum to many sources; analyzing their X-ray spectra can distinguish between pre-main sequence stars and AGN.

3. Analysis

3.1. Optical Properties of Chandra-detected Sources

Most of the 165 optically-detected X-ray sources define a clear sequence in the V/V-I color-magnitude diagram consistent with cluster membership. Figure 2 shows their positions (blue and green dots) with respect to all sources (grey dots) detected within 10' of the h Persei center ($\alpha_{2000} \sim 2^h19^m0^s$, $\delta_{2000} \sim 57^o8'35"$; see Bragg and Kenyon 2005). The cluster sources define a sequence from V,V-I $\sim$ 10,0 to V,V-I $\sim$ 24, 3.6, which is clearly separable from the background field star population (V $\gtrsim$ 15 + 3(V-I) for V-I $\gtrsim$ 1). Foreground stars are less numerous than either the cluster stars or the background. The brightest X-ray active star (V $\sim$ 8) is located beyond the plot limits.

To compare the magnitudes and colors of these stars with theoretical predictions, we overplot a best-fit isochrone (14 Myr), covering a range in masses from 15 $M_\odot$ to 0.6 $M_\odot$. We construct our isochrone for intermediate/low-mass stars ($\lesssim$ 1.4 $M_\odot$) by interpolating between the 12.6 Myr and 15.8 Myr isochrones from Baraffe et al. (1998). For more massive stars, we use the Geneva isochrones (Schaller et al. 1992; Meynet et al. 1993). On Figure 2, the Baraffe et al. and Geneva predictions meet at V $\sim$ 17, V-I $\sim$ 1.2. We adjust the isochrone to the distance and reddening of h Persei, assuming a distance modulus of 11.85 and E(B-V) $\sim$ 0.56 (Slesnick et al. 2002). For the rest of the paper, we label the isochrone constructed from tracks for high-mass stars from the Geneva group and intermediate/low-mass stars from Baraffe as the 'Geneva/Baraffe' isochrone.

The agreement between the predicted 14 Myr isochrone and the color-magnitude diagram for all h Per stars is exceptional. The isochrone accurately reproduces the cluster

locus from V, V-I = 10, 0 to V, V-I = 22.5, 2.8. At 14 Myr, this range corresponds to stars with masses $\gtrsim$ 0.6 $M_\odot$. Isochrones for 12.6 Myr and 15.8 Myr (not shown) also show fair agreement, though slightly younger (11.2 Myr) and older (17.8 Myr) isochrones provide a much poorer fit[6].

The vast majority (142/165) of Chandra-detected sources, especially those fainter than V=16, track this sequence extremely well. Many X-ray sources follow the isochrone from V $\approx$ 10 to V $\approx$ 21. A smaller number of much fainter X-ray sources (V $\sim$ 22–23, V-I $\sim$ 2.75-4) also track the locus of cluster stars. In addition to stars in the cluster, 12 foreground stars are X-ray active.

The X-ray active stars also follow clear sequences in an HR diagram (Figure 3, top panel) and in a diagram of V-I vs. spectral type (Figure 3, bottom panel). Aside from two early-type stars, there is a clear relation between color and spectral type in the lower panel of Figure 3. The X-ray active cluster sequence extends from V = 11, V-I= 0.4 to V = 23.5, V-I= 3.5. Over this range, h Persei sources have spectral types betweeen B2 and M0. Most detected X-ray active stars are F5-G5 stars with V=16-20 and V-I = 1-1.5. Early A stars with an intrinsic V-I $\sim$ 0 have an observed V-I $\sim$ 0.7 consistent with the mean cluster reddening of E(B-V) $\approx$ 0.56 (Bessel and Brett 1988; Slesnick et al. 2002).

Using the same upper and lower bounds in V/V-I to identify probable cluster members lacking X-ray detections, Chandra detects less than 10% of the h Persei cluster members. Within 8.5' of the center of the Chandra/ACIS coverage, 1,621 stars with V=11-22 lie within 0.75 mags of the isochrone. Of these stars, 130 have Chandra detections. These stars thus have optical colors and magnitudes consistent with cluster membership. The total fraction of X-ray detected cluster members with the same V, V-I limits and located within 8.5' of h Per is $\approx$ 8% (130/1621)[7]. In comparison, there are 1,764 stars within 8.5' of h Per that lie off the isochrone; 28 of these have Chandra detections. Therefore, $\approx$ 1.6% of nonmembers show evidence for X-ray activity (28/1764).

Converting from optical color and magnitude to stellar mass using the Geneva/Baraffe isochrone further constrains the fraction of cluster stars detected as a function of stellar mass. Very few high mass stars (M=2 $M_\odot$–5 $M_\odot$, V/V-I = 0.52 — 0.75) are detected (2.6%, 6/230). A slightly larger fraction of subsolar-mass stars (0.6 $M_\odot$–1 $M_\odot$, V-I =1.87 — 2.66) is detected (5.9%, 24/407). The detection rate for intermediate (1–2 $M_\odot$, V/V-I = 0.78 –

[6]A more detailed analysis of the success/failure of isochrones of different ages as well as isochrones from different groups will be included in an upcoming paper (Currie et al. 2008c)

[7]Given that the locus of giant stars crosses the cluster locus at V-I $\sim$ 1.7, we expect a small amount of contamination and thus some uncertainty in the true fraction of X-ray detected cluster members.

1.87) mass stars is highest, $\approx 11\%$ (97/911).

3.2. X-ray Luminosity and Fractional X-ray Luminosity

The vast majority of Chandra-detected sources with optical counterparts have optical magnitudes, colors, and spectra consistent with membership in h Persei. We now analyze the X-ray properties of likely h Persei members. X-ray active members are defined as those within 0.75 magnitudes of the 14 Myr isochrone[8]. We assume an extinction of E(B-V) $\sim$ 0.56, an age of 14 Myr, and a distance modulus of dM=11.85 for the cluster (Slesnick et al. 2002; Currie 2008b).

From these membership criteria, we investigate the X-ray luminosity function and the distribution of fractional X-ray luminosities. The X-ray luminosity function probes the absolute X-ray luminosity produced by the stellar chromosphere; the fractional X-ray luminosity function explores how X-ray luminous the star is compared to its photosphere. We compare these luminosity functions with the stars' dereddened colors and spectral types to investigate how they correlate with stellar properties.

The fractional luminosity, $L_x/L_\star$, is estimated from the observed L_x and the bolometric luminosity, $L_\star$, derived from the well-constrained age, reddening, and distance for h Persei. Assuming that all h Persei stars are $\sim$ 14 Myr old and have E(B-V) $\sim$ 0.56, we evaluated the expected spectral type, mass, and bolometric luminosity from V,V-I. The derived $L_\star$ for sources with V-I colors in between points on the Geneva/Baraffe isochrone grid is determined by interpolating between the points in theoretical $\log(L_\star)$ space.

3.2.1. X-Ray and Fractional X-Ray Luminosity Functions

Figure 4 shows the observed X-ray luminosity function for h Persei. The number counts peak at $\log(L_x$, ergs $s^{-1}) \sim 30.3$ (2×10^{30} ergs s^{-1}). To compare the peak to predictions for the limiting X-ray luminosity, we follow Feigelson et al. (2002, 2005) who compute the limiting L_x for a given exposure time, source distance, and n_H. For the full 0.5–8 keV band, $\log(L_{x,lim}$, ergs $s^{-1}) \sim 30.3$, in agreement with the observed peak.

We also show the distribution for the subset of stars with V-I=1.585-2.225 (dotted line).

[8]Technically, the upper limit should be larger than the lower limit because of binarity. For simplicity we make the upper and lower limits the same. Using a more restrictive lower limit (e.g. 0.3 magnitudes) does not affect our results.

At 14 Myr, these stars should have $M_\star \sim 0.9$–$1.2\ M_\odot$ and have G spectral types on the main sequence. The distribution for 0.9–1.2 $M_\odot$ stars is similar to the function for the entire population, though it lacks any stars with $\log(L_x) \geq 31$.

Because Chandra detects $\lesssim 10\%$ of all cluster stars, members without detections have lower X-ray luminosities. X-ray luminosity functions for both young and older clusters have many stars with $\log(L_x \text{ ergs s}^{-1}) << 30.3$ (e.g. Preibisch et al. 2005; Jeffries et al. 2006). Thus, the distribution of L_x shown in Figure 4 identifies the completeness limit in L_x, and the true X-ray luminosity function peaks at $\log(L_x \text{ ergs s}^{-1}) << 30.3$.

The distribution of $L_x/L_\star$ is peaked at $L_x/L_\star \sim 10^{-3.5}$ (Figure 4b). Because the vast majority of cluster stars are undetected, the true fractional X-ray luminosity function is likely peaked towards lower values. Three stars have a much higher fractional luminosity ($\approx 10^{-2}$), and several have a lower fractional luminosity of $\approx 10^{-3.8}$–$10^{-4.8}$.

Five sources– all early-type, high-mass stars– have an extremely low fractional luminosity of $\approx 10^{-6}$–10^{-7}. High-mass stars produce X-ray emission from wind shocks, not a magnetic dynamo as in solar/subsolar-mass stars, which yields far lower $L_x/L_\star$ (Stelzer et al. 2005). While an unseen low-mass companion could be responsible for the X-ray emission, this is an unlikely source for X-ray emission around high-mass stars in h Per. B5 stars with $L_x/L_\star \approx 10^{-6}$ typically have V $\approx$ 12; G stars with $L_x/L_\star \approx 10^{-3.5}$ have V $\approx$ 18. The bolometric corrections for B5 stars are BC $\approx$ -1.6; the corrections for G0 stars are BC $\approx$ -0.2. Therefore, B5 stars are $\approx$ 7.4 magnitudes brighter than G stars. Thus, the fractional X-ray luminosity of a G0 star in a G0/B5 binary needed to yield an observed $L_x/L_\star$ for the system of $\approx 10^{-6}$ is $\approx 10^{-3}$. Chandra detects only the most X-ray luminous G stars in h Per, which have $L_x/L_\star \leq 10^{-3}$. Because $\gtrsim 90\%$ of cluster G stars are less X-ray luminous, the likelihood that an unseen companion generates the X-ray flux observed from B stars is low.

Deeper X-ray observations would yield a better measure of the X-ray luminosity function and fractional X-ray luminosity function in h Per. In the younger Orion Nebula Cluster, Preibisch and Feigelson (2005) detect $\gtrsim 90\%$ of the 0.9-1.2 $M_\odot$ stars with typical $L_x/L_\star \sim 10^{-5}$ to 10^{-2} and a median $L_x/L_\star \approx 10^{-3}$ to $10^{-3.5}$. At the distance of h Persei, many of these stars would lie below the Chandra detection limit for G-type stars. Thus, the true X-ray and fractional X-ray luminosity functions are likely peaked at lower L_x and $L_x/L_\star$ values.

3.2.2. X-Ray Properties vs. Other Stellar Properties

The fractional X-ray luminosity correlates well with dereddened V-I color (Figure 5a). Most sources occupy a region bounded by V-I = -0.2-1.3 and $\log(L_x/L_\star) \sim$ -4 to -3. Bright cluster stars with blue V-I colors have weak X-ray emission compared to their photospheres; fainter stars with red V-I colors have relatively strong X-ray emission. Figures 5a and b show that the five extremely low fractional luminosity sources identified in Figure 4b are mostly B0-B5 stars. The lack of low-luminosity late-type stars is likely due to the Chandra sensitivity limits, which are shown as a dashed line. However, high-luminosity, early-type stars ($\log (L_x/L_\star) \sim$ -3) with V-I $\sim$ -0.2 – 0.3 are absent in h Persei and should have been easily detected.

Because brighter clusters stars at a given age have earlier spectral types than fainter cluster stars, the fractional X-ray luminosity of h Persei stars also correlates with spectral type (Figure 5b). Cluster stars with V-I $\sim$ -0.2 – 0.3 have spectral types between $\sim$ B0 and F5. Though h Persei contains thousands of stars with these spectral types, none of them have $L_x/L_\star \gtrsim 10^{-3.5}$.

In summary, Figure 5 shows that stars with small $L_x/L_\star$ ($\approx 10^{-7}$–10^{-5}) are early type (B/A), higher-mass stars while those with larger $L_x/L_\star$ ($\approx 10^{-5}$–10^{-3}) are intermediate type/mass stars (FGK). The B and A stars with X-ray emission are more massive than ≈ 2 $M_\odot$ at 14 Myr (Baraffe et al. 1998; Siess et al. 2000). The F–K stars with higher fractional luminosity have masses of $\approx$ 1–2 $M_\odot$. While Chandra likely detects only the most X-ray luminous cluster stars, these data provide some constraints on the X-ray luminosity function, specifically its upper envelope as a function of spectral type.

3.3. X-Ray Properties and IR Excess from Warm Debris Disks

The Double Cluster, h and χ Persei, contains the largest known population of warm debris disks (Currie et al. 2007a,b, 2008a; Currie 2008b). Ongoing terrestrial planet formation is the most likely source for the observed debris (Kenyon and Bromley 2004). Here we analyze the X-ray properties of Chandra-detected h Persei sources with warm debris disks. We focus on a) whether X-ray luminosity correlates with the amount of debris emission and b) identifying the X-ray luminosity of X-ray bright stars that are likely forming terrestrial planets.

Figure 6 shows the spectral types of Chandra sources vs. their observed K_s-[8] colors. X-ray bright stars with IRAC detections cover a wide range of spectral types (B0-K3). Most stars have spectral types earlier than G3 with K_s-[8] $\approx$ 0–0.3. To compare these colors

with the predicted colors of stellar photospheres, we add the locus of stellar K_s-[8] colors for B0–M0 stars from the Kurucz-Lejeune stellar atmosphere models using the SENS-PET tool available on the Spitzer Science Center website[9]. The locus of photospheric colors is nearly independent of spectral type from A stars through G stars (K_s-[8] ≈ 0), covering almost the entire spectral type range of Chandra sources.

Figure 6 also reveals four Chandra sources with IR excess emission from circumstellar dust. Currie et al. (2007a) identified 8 μm excess sources as those with K_s-[8] $\geq 0.4 + \sigma[8]$, where $\sigma[8]$ is the typical uncertainty in the 8 μm magnitude. For FGK stars with typical [8] $\sim$ 13.75, $\sigma[8] \sim 0.1$ (Currie et al. 2007a). Three stars have K_s-[8] colors redder than $\sim$ 0.5 and thus have 8 μm excess consistent with warm, terrestrial zone dust. A fourth star without a spectral type also has K_s-[8] > 0.5. Thus, at least 4 Chandra detections have excess emission at 8 μm.

The frequency of 8 μm excess emission among Chandra detections is comparable to the fraction in the entire cluster. The frequency of Chandra-detected stars with 8 μm excess is 4/123 (3.3% $\pm$ 1.7%. The frequency for Chandra-detected cluster members is 4/106 (3.7% $\pm$ 1.9%). For all F0-G5 stars in h and χ Persei, the fraction ranges from $\approx$ 4% to 8% (Currie et al. 2007a; Currie 2008b; Currie et al. 2008c). Given the small sample of X-ray bright stars with evidence for warm dust, the similarity in excess frequency between them and stars lacking Chandra detections should be considered a tentative result.

Figure 7 compares the K_s-[8] colors and X-ray luminosities for Chandra-detected cluster members. Most stars have $\log(L_x$, ergs $s^{-1}) \sim$ 30-30.8. Sources with red K_s-[8] colors do not identify a unique space in this plot. Three 8 μm-excess stars have $\log(L_x$, ergs $s^{-1}) \sim$ 30-30.4; a fourth has $\log(L_x$, ergs $s^{-1}) \sim 30.8$. The Spearman's rank test, a non-parametric measure of correlation, reveals that the distribution of L_x with K_s-[8] color is consistent with a random distribution (probability $\approx$ 23%, d=0.17).

Figure 7b shows the distribution of fractional X-ray luminosity with K_s-[8] color. Most IRAC-detected stars have $L_x/L_\star \sim 10^{-4.75}$–$10^{-2.75}$, which are typical of the X-ray bright population as a whole. Sources with 8 μm excess define a slightly more narrow distribution between $L_x/L_\star \sim 10^{-4}$–$10^{-2.9}$. According to the Spearman's rank test, the probability that $L_x/L_\star$ is not correlated with the K_s-[8] color is $\approx$ 0.89% (d=0.44). Thus, there is a 2–3σ correlation between X-ray flux and K_s-[8] color.

If this trend is real, the fractional X-ray luminosity probably does not affect the amount of debris emission. Currie et al. (2007a) and Currie et al. (2008c) find that intermediate-

[9]http://ssc.spitzer.caltech.edu/tools/senspet/

type (FG) stars more frequently have 8 μm excess than earlier stars. Intermediate-type stars also have higher fractional X-ray luminosities regardless of their circumstellar environment (Figure 5b). Therefore, the correlation between $L_x/L_\star$ and IR excess in Figure 7b is likely due to the intrinsically larger fractional X-ray luminosities and higher frequencies of warm dust for intermediate-type stars compared to early-type stars.

In spite of these results, we caution that they apply only to the *X-ray bright* population of stars with warm dust, not the population of disk-bearing sources as a whole. Other stars with warm dust located within the Chandra coverage must be more X-ray faint. Deeper Chandra data are required to more definitively probe the relationship between X-ray activity and IR excess.

3.4. X-ray Active Stars and Planet Formation in h Persei

If the 8 μm excess emission is due to active terrestrial planet formation, we can estimate the X-ray flux incident on forming planets given the temperature and location of the dust. Currie et al. (2008a) derive dust temperatures of $\approx$ 250-400 K for stars with 8 μm excess. Using the bolometric luminosity derived from the Geneva/Baraffe isochrone, we calculate the location of the dust assuming that dust grains are in radiative equilibrium with a temperature of $\approx$ 300 K. Derived dust locations range from $\approx$ 0.92 AU to 1.36 AU. From the location of the dust, we calculate the X-ray flux.

The incident X-ray flux on objects at the dust locations ranges from 1.53×10^2 ergs cm^{-2} s^{-1} to 2.20×10^3 ergs cm^{-2} s^{-1}. These levels are equal to or larger than the X-ray flux intercepted by the atmosphere of the hot Jupiter HD 209458b ($\sim$ 200 ergs cm^{-2} s^{-1} for $L_x \approx 1.1\times 10^{27}$ ergs s^{-1} at 0.045 AU, see Penz et al. 2008). Thus, a planet with a mass and radius similar to HD 209458b located at $\approx$ 1 AU from an X-ray luminous G star in h Per may experience similar rates of atmospheric erosion of up to $\approx 10^{10}$ g s^{-1} (Vidal-Madjar et al. 2003, 2004).

However, this level of atmospheric escape will not likely be sustained by any jovian planets in the terrestrial zones of h Per stars. Penz et al. (2008) indicate that the timescale for erosion of a significant fraction of a planet's mass is on the order of 100 Myr–1 Gyr. Over this timescale, the X-ray luminosity of the star will drop by several orders of magnitude (Preibisch and Feigelson 2005), which greatly reduces the rate of atmospheric escape.

4. Comparison With Other 1–100 Myr-old Chandra-observed Clusters

X-ray emission from young stars is most often associated with a magnetic dynamo, the "α-Ω" dynamo (Parker 1955; Babcock 1961; Barnes 2003). Differential rotation between an inner radiative core and an outer convective envelope drives the dynamo and powers chromospheric and coronal activity. For the Siess et al. (2000) isochrones of a 14 Myr-old cluster, we expect stars with outer convective envelopes to have spectral types later than $\sim$ G0 and stellar masses less than $\sim$ 1.4–1.5 $M_{\odot}$.

Early-type stars without convective envelopes do not produce a dynamo. Thus, these stars do not display stellar activity. However, many early-type stars have large X-ray luminosities with typical $L_x/L_\star \approx 4 - 400 \times 10^{-6}$ (e.g., Chlebowski et al. 1989; Stelzer et al. 2005). Shocks in high velocity stellar winds are the most likely source of X-ray emission in these stars (e.g., Feldmeier et al. 1997). For h Per, we expect wind emission to dominate chromospheric activity for stars with spectral types earlier than F0 and masses larger than $\sim$ 1.7 $M_{\odot}$.

Our results suggest that h Per contains both types of X-ray sources. Late-type stars likely powered by the α-Ω dynamo have $L_x/L_\star \lesssim 10^{-3}$ (Figure 5). Stars with spectral types earlier than $\sim$ F0 have fractional X-ray luminosities comparable to typical wind-driven sources. These fluxes are probably not produced by an unseen late-type companion (§3.2.1). Thus, shocks probably produce X-ray emission in these stars.

In this section, we compare the X-ray properties of h Per stars with X-ray active stars in younger and older clusters studied by Chandra and XMM-Newton. We divide our sample into "early" (B0-A3) and "intermediate" (FGK) type stars. Comparing h Per data with results for other clusters then provides constraints on the evolution of X-ray activity from intermediate-type stars and stellar wind-driven emission from early-type stars.

4.1. X-Ray Emission from Early-Type, High-Mass Stars (B0-A3)

Stelzer et al. (2005) divide early type X-ray active stars in the ONC into two groups. "Strong wind" stars have spectral types between O and B3 ($M \gtrsim 7$ $M_{\odot}$); "weak wind" stars have spectral types between B5 and A9 ($M \sim 2$–7 $M_{\odot}$). More than half (16) ONC early-type stars show clear evidence for X-ray emission. Orion stars with spectral types earlier than B3 are strong-wind stars with X-ray emission. About 64% of stars with spectral types between B5 and A9 are detected by Chandra.

At 14 Myr, assuming that the division between strong and weak-wind stars is set by stel-

lar mass, strong wind sources in h Per have spectral types earlier than B3. Weak wind stars have spectral types between B3 and A3. Chandra detects 9 h Per stars earlier than A3. None of these stars correspond to Be stars or candidate Be stars identified by Bragg and Kenyon (2005), Slesnick et al. (2002), and Currie et al. (2008a) and none show H_α emission characteristic of Be stars. Compared to the total population of B0-A3 stars within 8.5' of h Persei (where V-I $\leq$ 0.76), $\approx$ 4% are detected by Chandra. About 5.7% (6/106) of stars earlier than B3 (V-I $\lesssim$ 0.4) are detected, while 2.8% (6/217) of stars between B3 and A3 are detected. Other early-type cluster members either lack X-ray activity or have wind-driven X-ray luminosities less than $\approx 10^{30}$ ergs s^{-1}.

If the X-ray luminosity function for strong and weak-wind sources does not evolve from $\sim$ 1 Myr to $\sim$ 14 Myr, Chandra should have detected more weak wind and strong-wind h Per stars. Most (6/9) of the strong-wind stars in Orion have X-ray luminosities greater than the peak in L_x for h Per ($\sim$ 30.3 ergs s^{-1}). Similarly, 44% (3/7) of the weak-wind Orion stars have $L_x \geq$ 30.3 ergs s^{-1}. Although sensitivity limits for h Per observations preclude more detailed comparisons between the ONC and h Per luminosities for early-type stars, these results may suggest that the X-ray luminosities for early-type, high-mass stars at 14 Myr are weaker than they are at 1–2 Myr.

4.2. X-Ray Emission from $\lesssim$ 3 $M_\odot$ (FGK) Stars

Recent Chandra and XMM-Newton observations of young stellar clusters provide some constraints on the evolution of X-ray activity as a function of age and stellar mass for intermediate and low-mass stars. Independent of stellar mass, the typical fractional X-ray luminosity of 1 Myr-old stars in the ONC is $L_x/L_\star \approx 10^{-3}$ (Preibisch et al. 2005). For most young stars, the stellar rotational velocity increases with stellar mass, so $L_x/L_\star$ is independent of rotation (Preibisch and Feigelson 2005). By analogy with dynamo models for X-ray activity, the fractional X-ray luminosity for these stars is "saturated".

By $\approx$ 40-50 Myr, when intermediate-mass stars are on the main sequence, the stellar rotation rates of intermediate-mass have declined significantly (Prosser et al. 1996; Jeffries et al. 2006) and correlate better with X-ray flux. Stars in 50 Myr-old α Persei (Prosser et al. 1996, Fig. 5) show a systematic decline in $L_x/L_\star$ from 1.2 $M_\odot$ (B-V $\sim$ 0.6, G1 at 50 Myr) to 1.4 $M_\odot$ (B-V $\sim$ 0.4, F5 at 50 Myr). Cluster stars with masses $<$ 1.2 $M_\odot$ have $L_x/L_\star \sim 10^{-3}$ and thus have saturated X-ray emission. The distribution of $L_x/L_\star$ for NGC 2547 (38 Myr) shows a similar trend (Jeffries et al. 2006).

At ages $\gtrsim$ 100 Myr, subsolar-mass stars leave X-ray saturation. A wide range of stars

in the Pleiades ($M \leq 0.85$ $M_\odot$; K3 at 100 Myr) are intrinsically much fainter in X-rays than younger stars with the same mass. Finally, older field stars more massive than $\gtrsim 0.1$ $M_\odot$ also exhibit a decline in X-ray luminosity relative to younger clusters (Preibisch et al. 2005; Preibisch and Feigelson 2005). $L_x/L_\star$ ranges from $10^{-4.5}$ to 10^{-8} for solar-mass stars and 10^{-4} to $10^{-6.5}$ for subsolar-mass stars. The evolution of fractional X-ray luminosity vs. time shows a systematic decline and is consistent with the Skumanich braking track (Skumanich 1972, $L_x(t) \propto t^{-1/2}$).

At least two mechanisms are responsible for the evolution of $L_x/L_\star$ as a star contracts onto the main sequence. Rotational spin-down of a star reduces differential rotation at the radiative zone/convective zone boundary. Because differential rotation is responsible for driving the magnetic dynamo that produces X-ray emission, X-ray activity diminishes (Preibisch and Feigelson 2005).

Intermediate and high-mass stars also undergo significant structural changes as they evolve onto the main sequence. At the age of the Orion Nebula Cluster ($\sim$ 2 Myr), main sequence A stars (1.7–2.5 $M_\odot$) have spectral types between K1 and K4 (Siess et al. 2000). From 2 Myr to 30 Myr, $\sim$ 2 $M_\odot$ stars evolve in spectral type from K3 to G8 (5 Myr) to A3 (30 Myr). Main sequence F3 stars ($\sim$ 1.5 $M_\odot$) also undergo substantial changes in their internal structure, evolving from at $\sim$ K5 at 2 Myr, to K0 at 10 Myr, to F3 at 30 Myr. As stars evolve from G/K stars to A/F stars, their outer convective zones shrink and then disappear. The disappearance of their convective zones eliminates magnetic dynamo-induced X-ray activity (see Gilliland 1986; Stelzer et al. 2005; Preibisch and Feigelson 2005).

The X-ray detections for stars in h Per place useful constraints on both of these mechanisms. For h Per stars with masses $\sim$ 1.0–1.5 $M_\odot$, the maximum in log $L_x/L_\star$ (~ -2.8 to -3.0) is similar to the maximum observed in the ONC. Thus, there is no clear evidence for evolution in X-ray activity among 1–1.5 $M_\odot$ stars from $\approx$ 1 Myr to $\approx$ 14 Myr. Deeper Chandra data are required to probe the X-ray luminosity function of solar and subsolar-mass stars at smaller $L_x/L_\star$ and to constrain the evolution of their X-ray activity.

For more massive stars, there is clear evidence of evolution in X-ray activity. At $\approx$ 14 Myr, h Per stars with A0 to $\sim$ G0 spectral types have masses of 3 $M_\odot$ to 1.5 $M_\odot$. In the ONC, stars with these masses have a maximum log $L_x/L_\star \approx -2.7$ to -3.0. This maximum is independent of spectral type. In h Per, the maximum $L_x/L_\star$ clearly declines with spectral type. Our Chandra data yield an approximate relation $\log (L_x/L_\star)_{max} \approx -3.5-(M_\star/1.5M_\odot)$ for 1.5–3 $M_\odot$ stars. Thus, the fractional X-ray luminosity declines by a factor of roughly 30 (3) for 3 (1.5) $M_\odot$ stars.

Pre-main sequence stellar evolution is the simplest explanation for the evolution of log

$(L_x/L_\star)_{max}$ in 1.5-3 $M_\odot$ stars. As these stars evolve to the main sequence, their effective temperatures increase and they lose their convective envelopes. Stars with masses $\gtrsim 1.8$ $M_\odot$ have spectral types earlier than A7 and lack the convective atmospheres need for magnetic dynamo-driven X-ray activity. Thus, the X-ray activity of these stars may be similar to the weak wind sources at earlier spectral types. Stars with masses $\sim$ 1.5–1.8 $M_\odot$ have $\sim$ A7–G0 spectral types and much smaller convective atmospheres than G-type stars. These stars can drive weak dynamos and thus have larger fractional X-ray fluxes than earlier type stars. In both sets of stars, the decline in X-ray activity appears linked to changes in stellar structure as the stars evolve from K-type stars at $\sim$ 1–2 Myr to A-type stars on the main sequence.

Deeper Chandra data in h and χ Per and other 5–50 Myr-old clusters can test these conclusions. If stellar evolution is responsible for the decay of X-ray emission among more massive stars approaching the main sequence, this decay should be correlated with spectral type and uncorrelated with stellar rotation. Chandra observations of other young clusters are needed to see how $(L_x/L_\star)_{max}$ and the X-ray luminosity function of massive stars evolves with cluster age. If changes in the magnetic dynamo are responsible for the decay of X-ray activity among lower mass stars, deeper observations of (i) 10–20 Myr clusters (to measure the X-ray luminosity function for 0.1–1.5 $M_\odot$) stars) and (ii) 20–50 Myr clusters (to measure evolution in $(L_x/L_\star)_{max}$) are required.

5. Summary

We analyze the first Chandra survey of h Persei, part of the Double Cluster in Perseus. By matching Chandra-detected sources with optical/IR photometry and spectra, we identify X-ray active cluster members. Using the well constrained age and distance to h Per, we compute the bolometric luminosity of h Per stars and compare this luminosity to the derived X-ray luminosity. Comparing the X-ray luminosity and fractional X-ray luminosity to optical colors, spectra, and near-to-mid IR colors, we investigate the connection between X-ray activity and stellar/circumstellar properties.

These analyses yield the following results:

- There is a clear correlation of V, V-I with spectral type for the X-ray detections. The position of X-ray active stars relative to the observable cluster locus in V, V-I and their locus in V vs. spectral type shows that the vast majority of these stars are likely cluster members.

- Within the ACIS coverage, Chandra detects 8% of cluster stars more massive than $\approx$ 0.6 $M_\odot$. About 10% of 1–2 $M_\odot$ stars are detected while $\sim$ 3% of 2–5 $M_\odot$ stars and

$\approx$ 6% of 0.6–1 $M_\odot$ stars are detected. Thus, the sources detected by Chandra likely correspond to the bright end of a much larger population of X-ray active stars.

- The observed distribution of X-ray luminosities for Chandra-detected h Per sources peaks at $\log(L_x) \sim 30.3$. Because of the sensitivity limitations of Chandra, the true X-ray luminosity function likely peaks at a lower luminosity.

- The observed distribution of fractional X-ray luminosities correlates well with the V-I color and with spectral type. Early-type stars ($M \gtrsim 2\ M_\odot$) have a very small fractional luminosity ($\log(L_x/L_\star) <$ -4 to -5); $L_x/L_\star$ is much larger for G and K stars ($M \sim$ 1–1.4 $M_\odot$, ($\log(L_x/L_\star) \sim$ -4 to -3).

- There is no evidence for an X-ray saturated population of stars more massive than $\sim$ 1.5 $M_\odot$. In the Orion Nebula Cluster, the most X-ray active 1.5–3 $M_\odot$ stars have $\log(L_x/L_\star) \approx$ -3 independent of stellar mass. In h Persei, the most X-ray active 1.5–3 $M_\odot$ stars have $\log(L_x/L_\star) \approx$ -3.5 - $M_\star/1.5M_\odot$. Changes in stellar structure as these stars contract onto the main sequence likely play a critical role in this decline of X-ray activity.

- From our sample of X-ray bright stars, the presence of warm, terrestrial zone circumstellar dust is not correlated with X-ray luminosity. While stars with higher fractional X-ray luminosity are more likely to have warm dust, this trend is likely due to the higher frequency of warm dust around intermediate-type stars than around early-type stars.

- The warm circumstellar dust emission from X-ray active stars studied in this paper likely results from debris emission due to terrestrial planet formation (e.g. Currie et al. 2007a,b, 2008a,c). By computing the X-ray luminosity of these sources and assuming a dust temperature of $\approx$ 300 K, we derive an incident X-ray flux on forming terrestrial planets in systems with X-ray bright stars. This flux is very small compared to stellar irradiation and the radiated flux from terrestrial zone dust. Thus, X-ray emission is unlikely to affect the detectability of warm debris disks.

These data show that h Persei is important in understanding the evolution of X-ray activity for a range of stellar masses and provides connections between X-ray activity and terrestrial planet formation. Deeper Chandra observations of h Persei can better constrain the X-ray luminosity function to lower stellar masses, provide a much larger sample from which to compare X-ray activity and planet formation, and more clearly reveal the characteristic X-ray environment experienced by forming terrestrial planets. Deeper Chandra observations

will also yield enough counts for X-ray bright sources to study the evolution of coronal temperatures in intermediate-mass stars.

We thank Leslie Hebb and Simon Hodgkin for KPNO observing and Nelson Caldwell, Susan Tokarz, Perry Berlind, and Mike Calkins for scheduling, taking, and reducing the Hectospec spectra. We also thank Tom Barnes and Rebecca Cover for early work on this project. Comments from the referee, Leisa Townsley, greatly improved the manuscript. This work is supported by NASA Astrophysics Theory grant NAG5-13278, Spitzer GO grant 1320379, and NASA TPF Foundation Science grant NNG06GH25G. T.C. received support from a SAO Predoctoral Fellowship. N.R.E., B.D.S, and S.J.W. are supported by NASA contract numbers NAS8-03060 and G0-6007A.

REFERENCES

Aigrain, S., et al., 2007, MNRAS, 375, 29

Babcock, H. W., 1961, ApJ, 133, 572

Baliunas, S., et al., 1995, ApJ, 438, 269

Baraffe, I., et al., 1998, A&A, 337, 403

Baraffe, I., Selsis, F., Chabrier, G., Barman, T., Allard, F., Hauschildt, P., Lammer, H., 2004, A&A, 419, 13L

Barnes, S., 2003, ApJ, 586, 464

Bauer, F., et al., 2004, AJ, 128, 2048

Bessel, M., Brett, J., 1988, PASP, 100, 1134

Bragg, A. & Kenyon, S., 2005, AJ, 130, 134

Broos, P., et al., 2007, ApJS, 169, 353

Cash, W., 1979, ApJ, 228, 939

Chlebowski, T., Harnden, F. R., Jr., & Sciortino, S. 1989, ApJ, 341, 427

Currie, T., et al., 2007, ApJ, 659, 599

Currie, T., Kenyon, S., Rieke, G., Balog, Z., Bromley, B., 2007, ApJ, 663L, 105

Currie, T., Kenyon, S., Balog, Z., Bragg, A., Tokarz, S., 2007, ApJ, 669L, 33

Currie, T., Kenyon, S., Balog, Z., Rieke, G., Bragg, A., Bromley, B., 2008, ApJ, 672, 558

Currie, T., Kenyon, S. J., 2008, submitted

Currie, T., 2008, Ph.D. thesis, University of California-Los Angeles

Currie, T., Plavchan, P., Kenyon, S. J., 2008, ApJ, 688, 597

Currie, T., Irwin, J., Hernandez, J., et al., 2008, in prep.

Dahm, S., Simon, T., Proszkow, E. M., Patten, B. M., 2007, AJ, 134, 999

Daniel, K., Linsky, J., Gagne, M., 2002, ApJ, 578, 486

Evans, N. R., Seward, F., 2000, ApJ, 538, 777

Evans, N., et al., 2008, in prep.

Fabricant, D., et al., 2005, PASP, 117, 1411

Feigelson, E., Montmerle, T., 1999, ARA&A, 37, 363

Feigelson, E., et al., 2002, ApJ, 572, 335

Feigelson, E., et al., 2005, ApJS, 160, 379

Feldmeier, A., Puls, J., & Pauldrach, A. W. A. 1997, A&A, 322, 878

Freeman, P. E., Kashyap, V., Rosner, R., Lambd, D. Q., 2002, ApJS, 138, 185

Getman, K. V., et al. 2005, ApJS, 160, 319

Gilliland, R. L., 1986, ApJ, 300, 339

Glassgold, A., Najita, J., Igea, J., 1997, ApJ, 480, 344

Güdel, M., Guinan, E. F., & Skinner, S. L., 1997, ApJ, 483, 947

Güdel, M., 2004, A&A Rev, 12, 71

Güdel, M. et al. 2007, A&A, 468, 353

Habing, H. J., et al., 2001, A&A, 365, 545

Hernandez, J., et al., 2004, AJ, 127, 1682

Irwin, M., Lewis, J., 2001, New Astronomy, 45, 105

Irwin, J., Irwin, M., Aigrain, S., Hodgkin, S., Hebb, L., Moraux, E., 2007, MNRAS, 375, 1449

Jeffries, R., Evans, P. A., Pye, J. P., Briggs, K. R., 2006, MNRAS, 367, 781

Keller, S.C., et al., 2001, AJ, 122, 248

Kenyon, S., Bromley, B., 2004, ApJ, 602, 133L

Kenyon, S. J., Bromley, B., 2006, AJ, 131, 1837

Kenyon, S. J., Hartmann, L., 1995, ApJS, 101, 117

Lammer, H., Selsis, F., Ribas, I., Guinan, E. F., Bauer, S. J., Weiss, W. W., 2003, ApJ, 598, 124L

Lammer, H., et al., 2007, Astrobiology, 7, 185

Lyra, W., et al., 2006, A&A, 453, 101

Meynet, G., Merilliod, J-C., Maeder, A., 1993, A&AS, 98, 477

Micela, G., et al., 1985, ApJ, 292, 172

Micela, G., et al., 1999, A&A, 341, 751

Miller, G., Scalo, J., 1979, ApJS, 41, 513

Noyes, R., Hartmann, L., Baliunas, S., Duncan, D., Vaughan, A., 1984, ApJ, 279, 763

Parker, E. N., 1955, ApJ, 122, 293

Penz, T., Micela, G., Lammer, H., 2008, A&A, 477, 309

Pallavicini, R., Golub, L., Rosner, R., Vaiana, G., Ayres, T., Linsky, J., 1981, ApJ, 248, 279

Patten, B., Simon, T., 1996, ApJS, 106, 489

Pizzolato, N., Maggio, A., Micela, G., Sciortino, S., Ventura, P., A&A, 397, 147

Preibisch, T., Zinnecker, H., 2002, AJ, 123, 1613

Preibisch, T., et al., 2005, ApJS, 160, 401

Preibisch, T., Feigelson, E., 2005, ApJS, 160, 390

Prosser, C. F., et al., 1996, AJ, 112, 1570

Randich, S., Schmitt, J., Prosser, C., Stauffer, J., 1996, A&A, 305, 785

Ryter, C. E., 1996, Ap&SS, 236, 285

Schaller, G., Schaerer, D., Meynet, G., Maeder, A., 1992, A&AS, 96, 269

Siess, L., et al., 2000, A&A, 358, 593

Skumanich, A, 1972, ApJ, 171, 565

Shu, F., Shang, H., Lee, T., 1996, Science, 271, 1545

Slesnick, C., Hillenbrand, L., and Massey, P., 2002, ApJ, 576, 880

Spitzbart, B., et al., 2008, in prep.

Stelzer, B., et al., 2005, ApJS, 160, 557

Thommes, E., Matsumura, S., and Rasio, F., 2008, Science accepted, arXiv:0808.1439

Vidal-Madjar, A., Lecavalier des Etangs, A., Desert, J.-M., et al., 2003, Nature, 422, 143

Vidal-Madjar, A., Lecavalier des Etangs, A., et al., 2004, ApJ, 604, 69L

Vuong, M. H., Montmerle, T., Grosso, N., Feigelson, E. D., Verstraete, L., & Ozawa, H. 2003, A&A, 408, 581

Wetherill, G., Stewart, G., 1993, Icarus, 106, 190

Weisskopf, M. C., et al., 2002, PASP, 114, 1

This preprint was prepared with the AAS LaTeX macros v5.2.

Table 1. Chandra/ACIS Detections

ID	RA	DEC	Raw Counts	Net Counts	HR1	HR2	HR3	n_H 10^{22} cm^{-2}	kT (keV)	σ(kT) (keV)	Flux$_{unabs.}$ ergs s^{-1} cm^{-2}	Flux$_{abs.}$ ergs s^{-1} cm^{-2}	Red.(χ^2)
1	34.9295	57.1005	34	31.7	-0.1593	-0.2562	0.0054	0.3	3.903	-999	5.49E-15	3.81E-15	0.572
2	34.9195	57.0918	6	3.2	-999	-999	-999	0.3	0.216	0.044	9.38E-15	1.26E-15	0.302
3	34.9152	57.0597	28	20.3	-999	-0.7477	-999	0.3	0.913	0.429	4.25E-15	1.84E-15	0.593
4	34.9039	57.0547	26	20	-0.5233	-0.0469	-0.6703	0.3	1.54	0.641	4.01E-15	2.15E-15	0.487
5	34.8843	57.1138	17	15.2	-0.7636	-0.6217	-0.4442	0.3	1.599	0.14	2.54E-15	1.38E-15	0.532

Note. — Sources detected by Chandra/ACIS. The hydrogen column, n_H, is fixed at $3\times$ 10^{21} cm^{-2} based on the well-constrained reddening to h Persei. The temperature (kT), normalization, and x-ray flux (Flux$_{unabs.}$) are determined by Sherpa.

Table 2. Catalog of Chandra sources with Optical Counterparts

ID	RA	DEC	Net Counts	σ(Net Counts)	log(L_x) ergs s^{-1}	ST	σ(ST)	J	H	K_s	[3.6]	[4.5]	[5.8]	[8]	V	σ(V)	I	σ(I)
3	34.9151	57.0597	20.3	5.83	30.47	99	99	14.026	13.536	13.340	13.144	13.121	13.151	13.425	16.512	0.001	15.050	0.001
4	34.9035	57.0546	20.0	5.74	30.45	48.6	1.4	15.883	15.235	14.932	14.870	99	99	99	19.094	0.004	17.309	0.003
5	34.8843	57.1137	15.2	4.36	30.25	30.5	2.2	13.897	13.521	13.473	13.246	99	13.425	13.274	15.872	0.001	14.785	0.001
7	34.8709	57.1545	10.3	2.96	30.17	13.2	2	11.044	10.975	10.970	10.920	10.924	11.085	10.984	11.814	0.001	11.174	0.001
8	34.8705	57.1777	17.2	4.94	30.39	99	99	15.624	14.951	14.595	14.482	14.462	99	99	18.771	0.003	16.982	0.003

Note. — Chandra sources with optical counterparts. The spectral types (ST) correspond to numerical spectral types: 10=B0, 20=A0, 30=F0, 40=G0, and 50=K0, etc. The uncertainties in spectral types (σ(ST)) are given in subclasses. Sources without spectral types and/or photometry in a given filter have entries denoted with '99'.

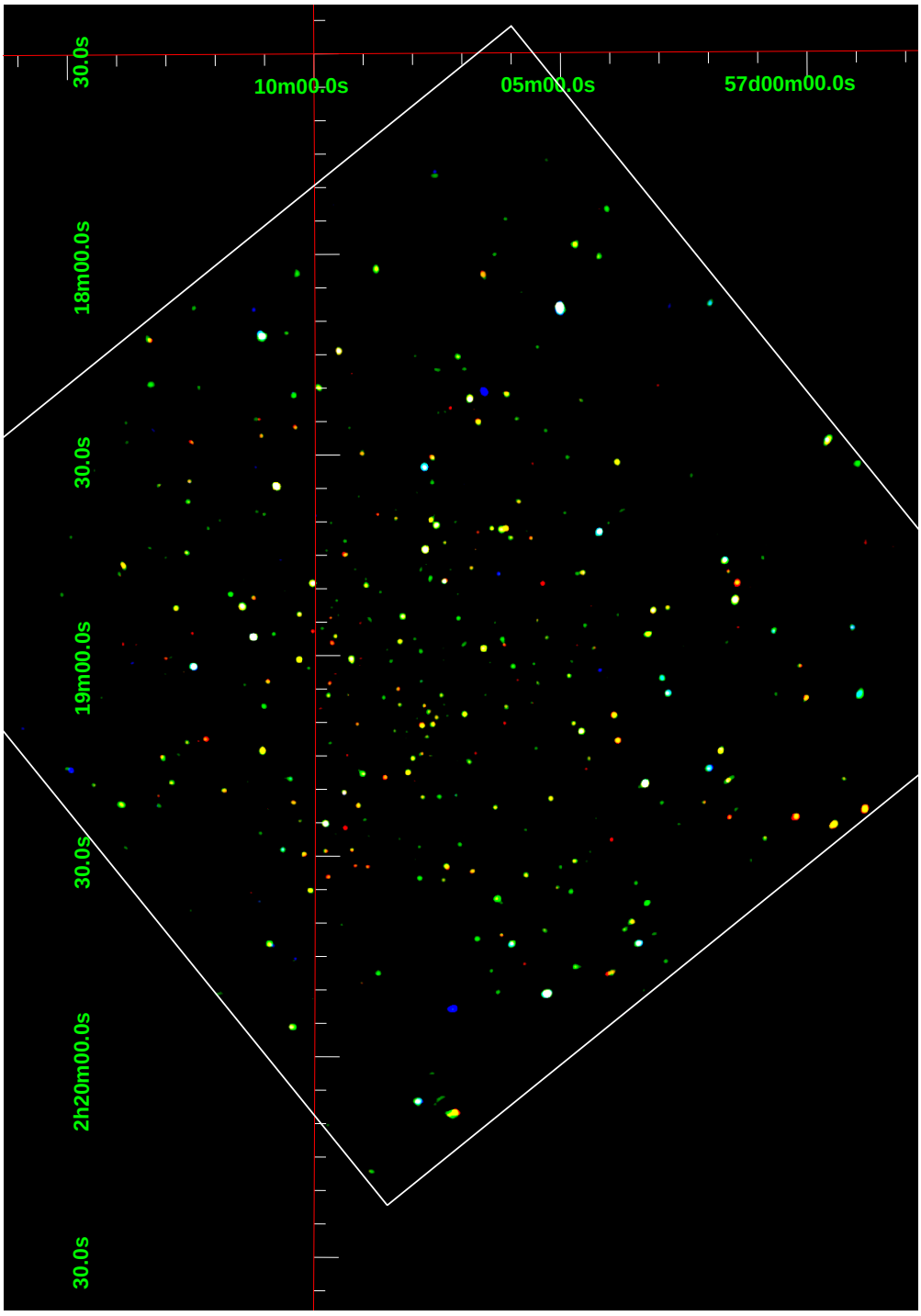


Fig. 1.— False-color image of the Chandra field binned by 4 pixels and convolved with a 3-pixel gaussian. The center of h Persei is at $\alpha_{2000} \sim 2^h18^m56.4^s$, $\delta_{2000} \sim 57^o8$'25" according to Bragg and Kenyon (2005).

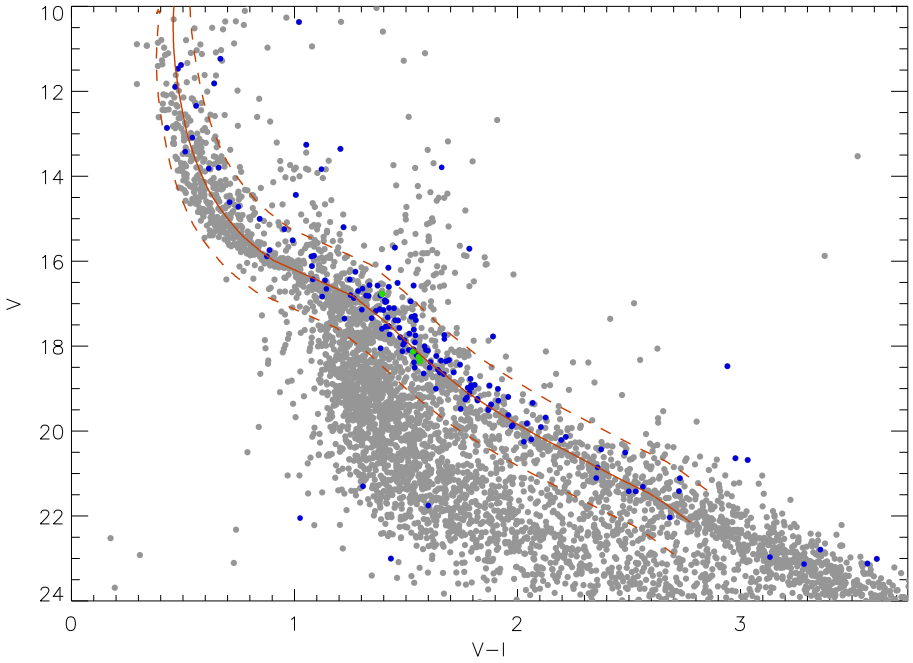


Fig. 2.— V/V-I color-magnitude diagram with h Persei sources within 10' of the cluster center (grey dots). Blue dots correspond to Chandra-detected sources with K_s-[8] $\leq$ 0.5 and light-green dots correspond to Chandra-detected sources with K_s-[8] $\geq$ 0.5. The solid line denotes the best-fit (14 Myr) isochrone using the Geneva/Baraffe models with 0.75 magnitude upper and lower limits. The lower mass limit for the isochrone (V=22, V-I=2.8) corresponds to 0.6 $M_\odot$. Most Chandra sources with optical counterparts follow the predicted isochrone.

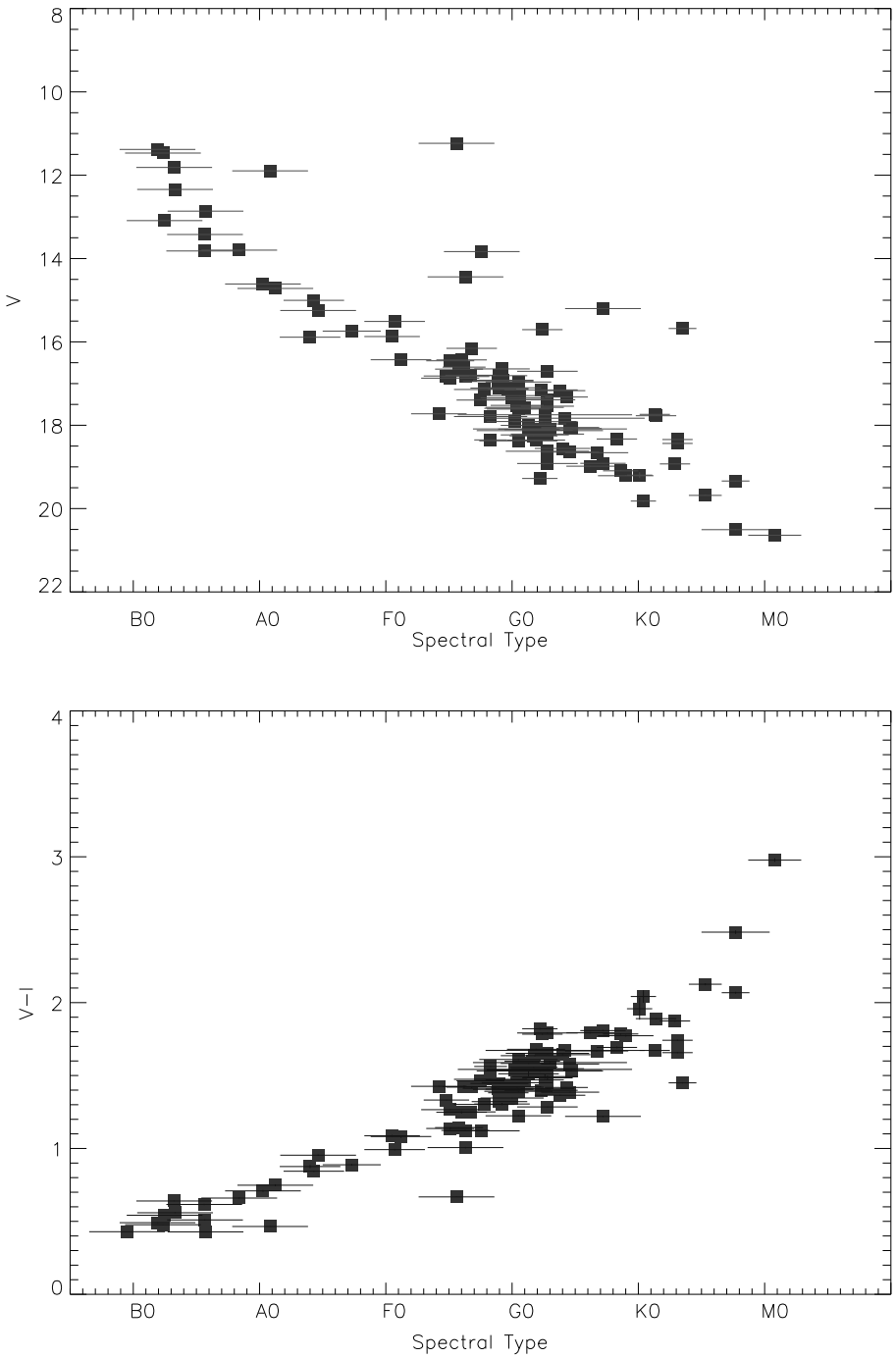


Fig. 3.— V vs. spectral type (top panel) and V-I vs. spectral type (bottom panel) for Chandra-detected sources. The sequence of X-ray active stars clearly traces a locus in both diagrams. We overplot error bars for both V-band photometry and spectral type. Photometric errors are too small to see for most sources.

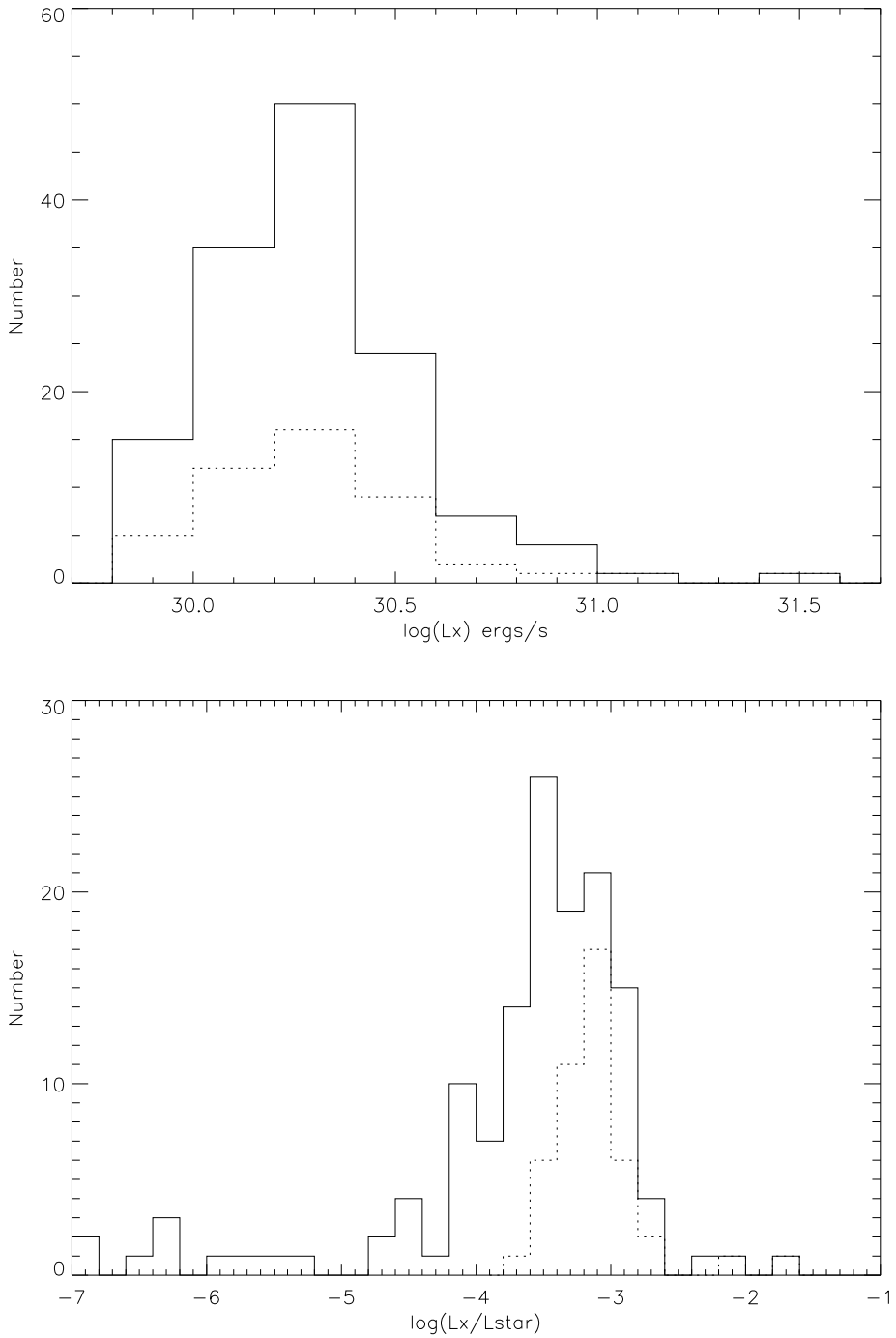


Fig. 4.— Observed distributions of L_x and $L_x/L_\star$ for the h Per stars with optical/IR counterparts. (top) Histogram of the L_x for Chandra sources. The number counts peak at $\log(L_x)$ = 30.3 ergs s^{-1} for all stars (solid line) and at $\log(L_x) \sim$ 30-30.4 ergs s^{-1} for stars with M $\approx$ 1 $M_\odot$ (dashed lines). (bottom) Histogram of the fractional X-ray luminosity. The fractional luminosity is peaked at $\log(L_x/L_\star) \sim$ -3.5 for all stars (solid line) and at -3.2 for stars with M $\sim$ 1 $M_\odot$ (dashed line). X-ray radiation contributes $\sim 10^{-4}$–10^{-3} of the total stellar flux for most h Per stars. In both plots, Chandra sensitivity limits preclude us from fully sampling the entire X-ray luminosity function and fractional X-ray luminosity function.

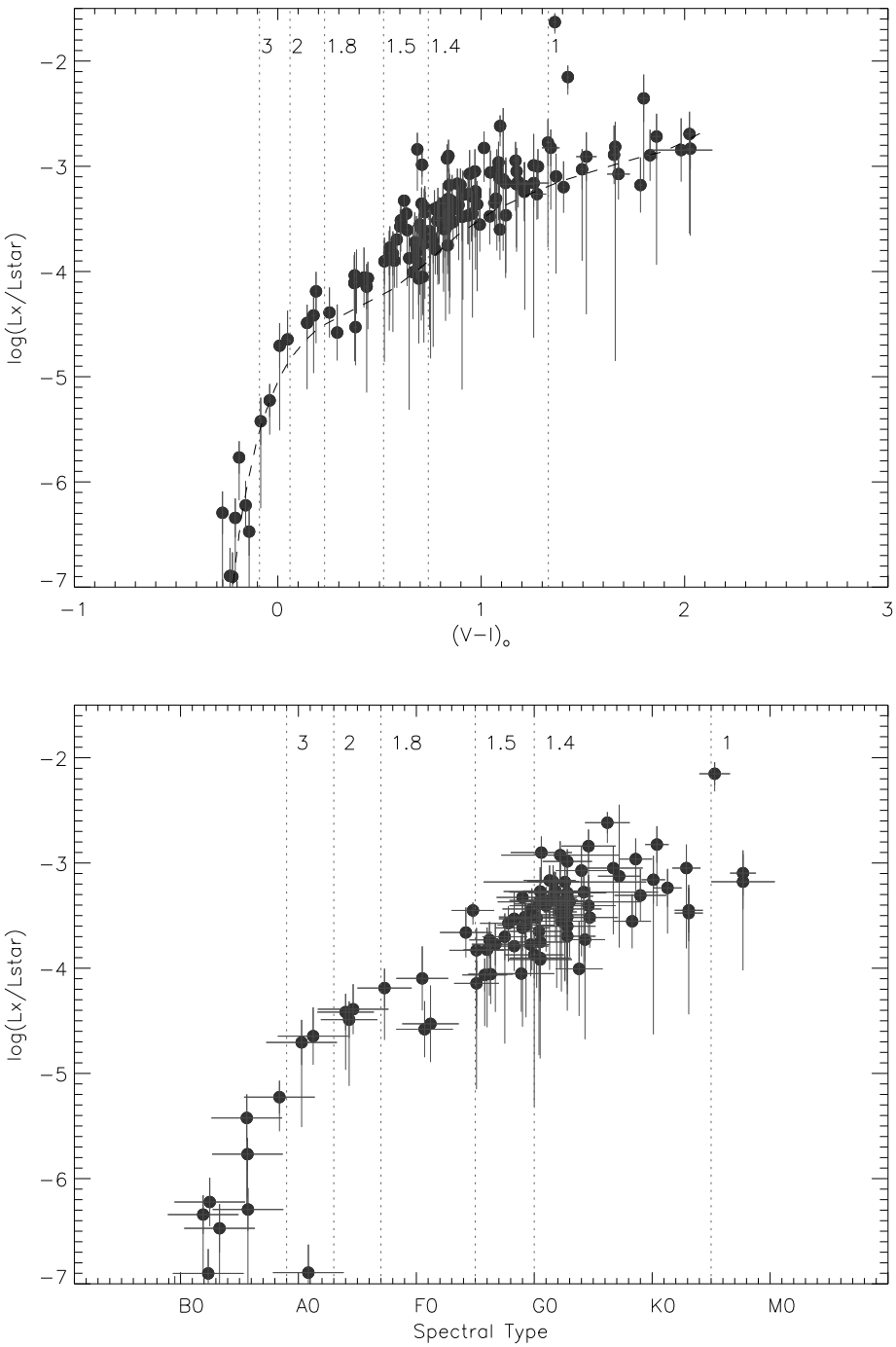


Fig. 5.— Fractional X-ray luminosity as a function of dereddened V-I color (top panel) and spectral type (bottom panel). The X-ray luminosity defines a clear sequence from bluer stars with a low luminosity to redder stars with a higher luminosity. The nominal Chandra detection limit determined from Feigelson et al. (2005) is shown as a dashed line. Uncertainties for luminosity and fractional luminosity shown in both panels are determined from the Sherpa fits; uncertainties for the color and spectral type are also shown. Stellar masses for 14 Myr-old stars from Baraffe et al. (1998) for low-mass stars and Siess et al. (2000) for high-mass stars are indicated by vertical dotted lines.

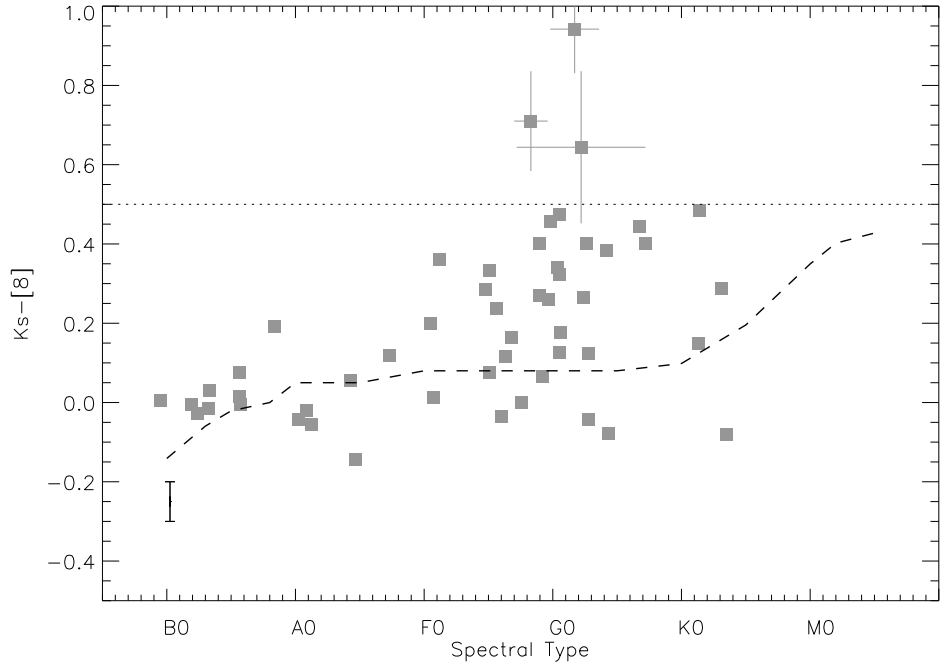


Fig. 6.— K_s-[8] vs. spectral type for optically-detected Chandra sources consistent with cluster membership. The dashed line shows the locus of photospheric K_s-[8] colors from the SENS-PET tool (available on the Spitzer Science Center website) using the Kurucz-Lejeune stellar atmosphere models. The dotted line shows the division between photospheric and excess sources adopted here. Error bars for excess sources are shown explicitly; the error bar in the lower left corner indicates a typical uncertainty in the K_s-[8] color ($\sigma \sim 0.1$) for all sources. Cooler stars have a larger range of K_s -[8] colors. At least three of the X-ray active F and G stars have red 2MASS-IRAC colors consistent with warm, terrestrial zone dust emission.

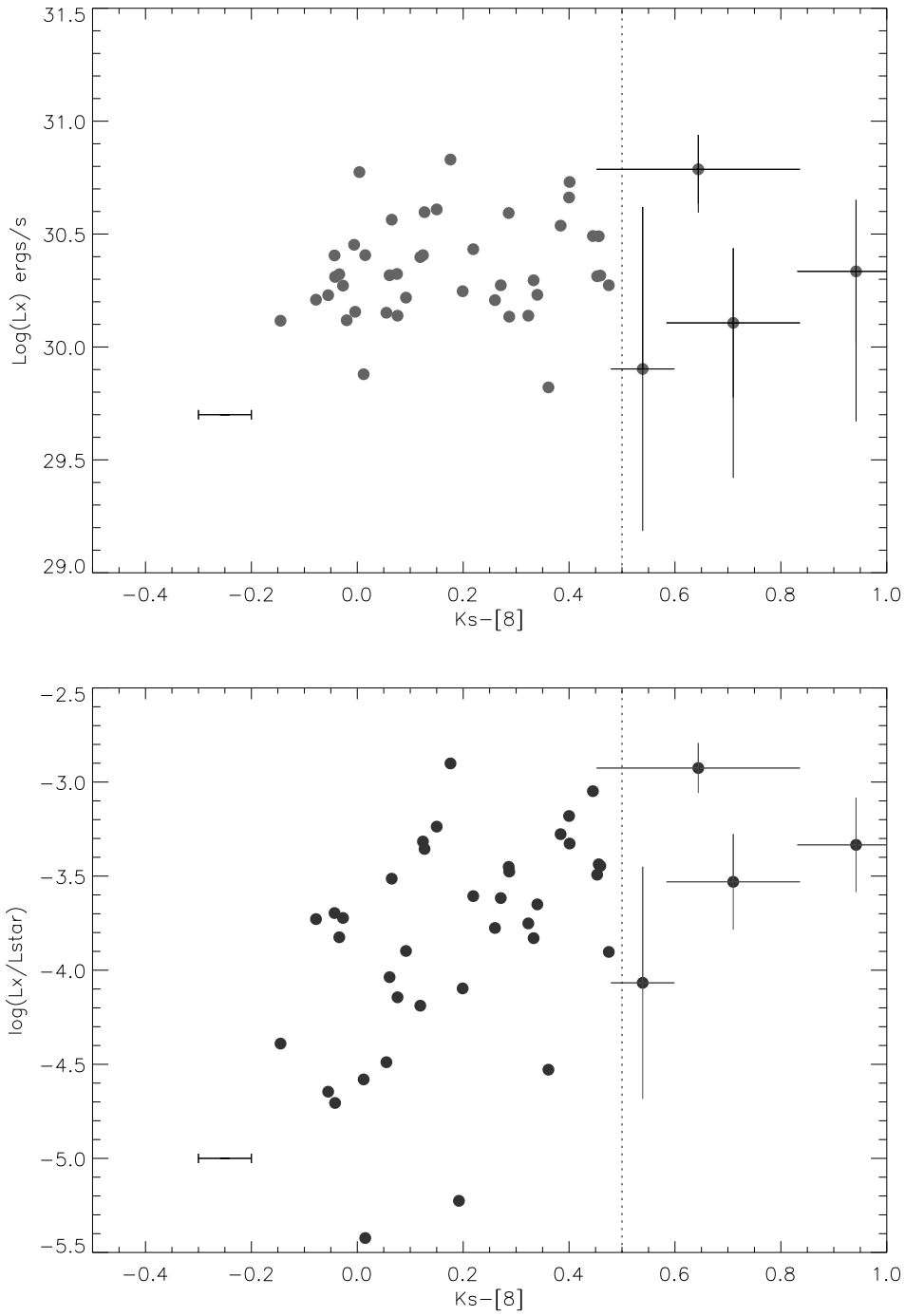


Fig. 7.— The relationship between X-ray luminosities and IR excess emission. L_x vs. K_s-[8] (top panel) and $\log(L_x/L_\star)$ vs. K_s-[8] (bottom panel) for sources detected by Chandra, 2MASS, and the $8\mu m$ filter in IRAC. The dotted line corresponds to the division between excess emission and no excess emission. The uncertainties in (fractional) luminosity and photometry are shown for excess sources; the typical K_s-[8] uncertainty is also shown (lower left-hand corner). Most sources lie in a distribution between K_s-[8] =0 and 0.4. About 3-4 stars may have IRAC excess emission indicative of warm, terrestrial zone dust.